Lamellar Stacking in Three-Dimensional Crystals of Ca^{2+}-ATPase from Sarcoplasmic Reticulum

Gang-Won Cheong,* Howard S. Young,* Haruo Ogawa,‡ Chikashi Toyoshima,§ and David L. Stokes*
*Skirball Institute of Biomolecular Medicine, New York University Medical Center, New York, New York 10016 USA; ‡Department of Biological Sciences, Tokyo Institute of Technology, Nagatsuta, Yokohama 22, Japan; and §Institute of Molecular and Cellular Biosciences, University of Tokyo, Bunkyo-ku, Tokyo 113, Japan

ABSTRACT Electron microscopy of multilamellar crystals of Ca^{2+}-ATPase currently offers the best opportunity for obtaining a high-resolution structure of this ATP-driven ion pump. Under certain conditions small, wormlike crystals are formed and provide views parallel to the lamellar plane, from which parameters of lamellar stacking can be directly measured. Assuming that molecular packing is the same, data from these views could supplement those obtained by tilting large, thin platelike crystals. However, we were surprised to discover that the lamellar spacing was variable and depended on the amount of glycerol present during crystallization (20% versus 5%). Projection maps (*h*,0,*l*) from these wormlike crystals suggest different molecular contacts that give rise to the different lamellar spacings. Based on an orthogonal projection map (*h*,*k*,0) from collapsed, wormlike crystals and on x-ray powder patterns, we conclude that molecular packing within the lamellar plane is the same as that in thin, platelike crystals and is unaffected by glycerol. Finally, the orientation of molecules in the lamellar plane was characterized from freeze-dried, shadowed crystals. Comparing the profile of molecules in these multilamellar crystals with that previously observed in helical tubes induced by vanadate gives structural evidence of the conformational change that accompanies binding of calcium to Ca^{2+}-ATPase.

INTRODUCTION

The calcium pump from sarcoplasmic reticulum (Ca^{2+}-ATPase) is an important member of the family of P-type ion pumps, which also includes Na^+/K^+-ATPase and H^+/K^+-ATPase (Green, 1992). Indeed, Ca^{2+}-ATPase has been the subject of a vast number of studies employing diverse methods, and a great deal is therefore known about its kinetics and ligand binding (Bigelow and Inesi, 1992). Despite its large size (115 kDa), extensive site-directed mutagenesis has identified many important amino acids, and in most cases, specific effects of mutations on the reaction cycle have been characterized (Andersen and Vilsen, 1994). The folding of the sequence into a three-dimensional structure has been addressed both by predictive algorithms and by direct experiment. Thus, elaborate models have evolved that predict 1) the number of transmembrane crossings (MacLennan et al., 1985), which are assumed to be helical, 2) the relationship of these helices to ATP-binding and phosphorylation domains (Brandl et al., 1986), and 3) even folding of secondary structure within these domains (Taylor and Green, 1989). Much attention has been focused on the arrangement of transmembrane helices, which are thought to contain the calcium-binding sites (Clarke et al., 1989). In particular, the ten predicted transmembrane helices have been recently fitted into a low-resolution structure (Stokes et al., 1994). In addition, the detailed liganding of two calcium ions by side chains from six specific residues (identified by site-directed mutagenesis) has been modeled based on the calcium-binding site of thermolysin, which uses six analogous residues for cooperative binding of two calcium ions (Inesi et al., 1994).

Electron microscopy has been used to address directly the structure of Ca^{2+}-ATPase but has not yet been able to provide a level of detail to match the models. Two-dimensional crystals of Ca^{2+}-ATPase can be formed within the membrane of the sarcoplasmic reticulum by either lanthanides (Dux et al., 1985) or vanadate (Dux and Martonosi, 1983), and the latter have been used for three-dimensional reconstruction of both negatively stained and frozen-hydrated specimens. Reconstructions of negatively stained specimens (Castellani et al., 1985; Taylor et al., 1986) showed the shape of the cytoplasmic head of the molecule at 25–30 Å resolution, which had previously been shown by low-angle x-ray diffraction to represent ~65% of the molecular mass (Herbette et al., 1985). This shape has been used as a template for structure prediction and for considering results of fluorescence energy transfer between intramolecular sites (Bigelow and Inesi, 1991). A reconstruction of frozen-hydrated crystals at 14 Å resolution (Toyoshima et al., 1993) revealed transmembrane and luminal parts of the molecule in addition to defining the domain structure within the cytoplasmic head. The transmembrane portion of this structure is large enough to accommodate ten α helices (Stokes et al., 1994), although the resolution of the reconstruction is too low to see them directly.

Another crystal form (Dux et al., 1987; Pikula et al., 1988) provides an opportunity to obtain a higher resolution structure in which helices could be directly observed. These

Received for publication 31 October 1995 and in final form 19 January 1996.

Address reprint requests to Dr. David L. Stokes, Skirball Institute, New York University Medical Center, 540 First Avenue, New York, NY 10016. Tel.: 212-263-1580; Fax: 212-263-1678; E-mail: stokes@saturn.med.nyu.edu.

Dr. Cheong is no longer at the Skirball Institute of Biomolecular Medicine, New York Univerisity Medical Center, New York, New York 10016.

0006-3495/96/04/1689/11 $2.00

small, three-dimensional crystals are grown from affinity-purified, detergent-solubilized Ca^{2+}-ATPase and have been shown to diffract beyond 4 Å resolution in the electron microscope (Stokes and Green, 1990a; Shi et al., 1995). The crystals are composed of a stack of lamellae, and each lamella contains a bilayer of detergent and lipid (~1:1 weight ratio) with Ca^{2+}-ATPase molecules protruding from either side (Fig. 1). Depending on the detergent-to-lipid ratio, these crystals adopt different morphologies: high detergent-to-lipid ratios produce rather small, wormlike crystals with a large number of lamellae, whereas low ratios produce much larger, platelike crystals with relatively few lamellae (3–10). Because of their respective shapes, these crystals lie in different orientations on the carbon support, thus offering orthogonal views of what has been presumed to be the same crystal lattice. Based on images of both crystal morphologies in negative stain, the stacking of lamellae appeared to be well ordered, and the observed symmetries were consistent with the space group C2. Although the angle between the *a* and *c* unit cell axes (β) is unconstrained in C2, it appeared to be close to 90°; however, this angle could not be accurately determined, because of distortions arising from the use of negative stain. The unit cell spacing normal to the lamellae (*c*) was measured as 164 Å by low-angle x-ray diffraction of fully hydrated crystals (Stokes and Green, 1990b).

Our strategy for three-dimensional reconstruction of this crystal form involves tilting the thin, platelike crystals to build up a three-dimensional data set. This is analogous to methods used for unilamellar, two-dimensional crystals (e.g., bacteriorhodopsin; Amos et al., 1982), except that, in our case, there exists a three-dimensional lattice of reflections in Fourier space rather than the two-dimensional array of lattice lines from two-dimensional crystals. To determine the (*h,k,l*) indices of specific reflections sampled at a given tilt angle and tilt axis, we must know the precise geometry of the unit cell. The current work was therefore initiated to determine more reliable values for the angle β and for the unit cell spacing along the *c* crystal axis. In addition, we have further investigated the packing of molecules in the unit cell and compared this packing in platelike and in wormlike crystals. If the packing is identical, then wormlike crystals would provide data along the lamellar axis (*c**), which cannot be obtained by simply tilting the platelike crystals, because of the physical limitation of 60° tilt in the electron microscope. Inclusion of these data would significantly improve the resolution of the resulting structure normal to the lamellar plane, typically a weakness in tilt reconstructions (Henderson et al., 1990; Unger and Schertler, 1995).

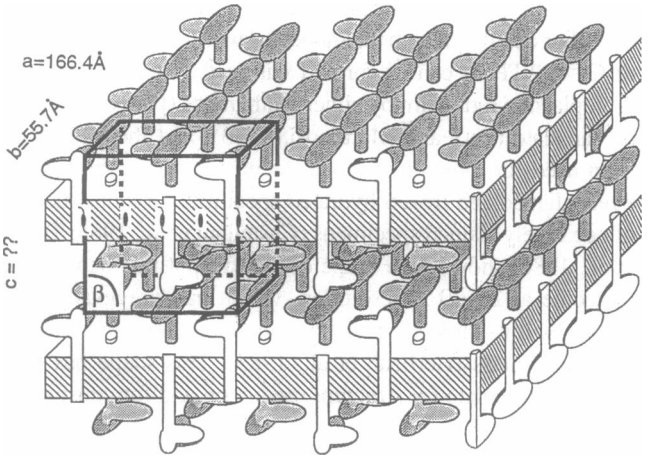

FIGURE 1 Packing model for multilamellar crystals of Ca^{2+}-ATPase. The planar, hatched regions represent bilayers containing lipid, detergent, and Ca^{2+}-ATPase molecules protruding from both sides. The molecules adopt a centered lattice within the lamellae; the dimensions and symmetry have previously been documented by electron microscopy of platelike crystals (Stokes and Green, 1990a,b; Taylor et al., 1988). The stacking of lamellae has been observed in negatively stained crystals, but both the spacing (*c*) and the angle (β) are uncertain in hydrated crystals. Furthermore, the specific orientation of the molecule in the lamellar plane is uncertain, although the orientation depicted, with the nose parallel to the *a* axis, was suggested on the basis of projection maps. Adapted from a diagram by Stokes and Green (1990b).

MATERIALS AND METHODS

Preparation and crystallization of Ca^{2+}-ATPase

Sarcoplasmic reticulum was prepared from the white, leg muscle of rabbit according to the method of Eletr and Inesi (1972). Ca^{2+}-ATPase was purified by affinity chromatography, and crystallization was carried out in microdialysis cells as described by Stokes and Green (1990b). Briefly, 1–3 mg/ml egg yolk phosphatidylcholine was added to the column eluant containing 2 mg/ml Ca^{2+}-ATPase, 1 mg/ml $C_{12}E_8$, 1 mM $MgCl_2$, 1 mM $CaCl_2$, 10 mM 3-(*N*-morpholino)propanesulfonic acid (pH 7), and 4 mM ADP. This solution was dialyzed against a crystallization buffer containing 20% glycerol, 100 mM KCl, 10 mM $CaCl_2$, 3 mM $MgCl_2$, 20 mM 2-(*N*-morpholino)ethanesulfonic acid (pH 6.0), 1 mM NaN_3, and 5 mM dithiothreitol at 4°C, and crystals formed after 1–4 weeks. Depending on the amount of lipid present, we obtained either large, flat, platelike crystals or long, wormlike crystals. In the case of wormlike crystals, a dialysis solution with 5% glycerol was also used for some crystallizations.

Electron microscopy

For freeze-drying and shadowing, the thin, platelike crystals were first adsorbed to carbon-coated, glow-discharged grids and washed with three consecutive drops of 0.1–0.2% uranyl acetate. The excess solution was blotted from the grids with filter paper before they were frozen in a slush of liquid ethane. The frozen grids were then transferred to a Balzers 300 (BalTec Productions, Middlebury, CT) freeze-etch machine and freeze-dried at −100°C for 1 h. Once dry, the temperature was reduced to −150°C, and the specimen was shadowed unidirectionally with Pt/C at a fixed angle of 20°. The grids were then examined directly in the electron microscope, without cleaning the replicas. Crystal features were not visible unless uranyl acetate was present during washing, similar to previous results with freeze-dried sarcoplasmic reticulum from scallop (Castellani et al., 1989). The uranyl acetate may therefore act to stabilize molecules on the surface of crystals when the mother liquor is replaced with a solution of very low ionic strength, which is required to minimize salt deposits after freeze-drying. However, the concentrations of uranyl acetate used were apparently not enough to generate negative stain contrast because maps, both from averaged and from individual images, did not show a contribution from molecules internal to the crystal (see discussion of Figs. 5 and 6

in Results). To reduce variability due to different directions of shadowing, we selected images for averaging that were shadowed approximately parallel to the *b* crystal axis.

For frozen-hydrated microscopy, solutions containing long, wormlike crystals were placed on glow-discharged grids covered with a perforated carbon film. The excess solution was removed by blotting with filter paper from the opposite side of the grid (Toyoshima, 1989), thus drawing the solution through the holes and concentrating crystals on the carbon film. Grids were then frozen in a liquid ethane slush and kept frozen in a Philips (Mahwah, NJ) 400T microscope with a cryoholder (Gatan Corp., Pleasanton, CA). Because solutions with 20% glycerol were too viscous to provide sufficiently thin films of ice after blotting, the crystals were first diluted ~10-fold with 100 mM KCl, 10 mM $CaCl_2$, 3 mM $MgCl_2$, and 20 mM 2-(*N*-morpholino)ethanesulfonic acid (pH 6.0); crystals grown in 5% glycerol were treated in the same way, except that the dilution was somewhat less (5–10-fold). Two images were recorded on Kodak SO163 film of each crystal, with defocus values of ~8000 Å and ~1.6 μm, using minimum electron doses (5–10 electrons/Å^2 for each image).

Image analysis

Images were selected based on optical diffraction and were digitized at 50-μm intervals (10 Å sampling) in the case of shadowed, freeze-dried crystals, and at 20-μm intervals (4.3 Å sampling) in the case of frozen-hydrated crystals. For freeze-dried crystals, defects in the crystal lattice were corrected with a suite of programs developed at the MRC Laboratory of Molecular Biology (Henderson et al., 1986). Even though these crystals only diffracted to low resolution, this "unbending" significantly improved the sharpness of Fourier reflections and thus made determination of amplitudes and phases more accurate. For all three groups of crystals (freeze-dried platelike crystals and wormlike crystals grown either in 20% or in 5% glycerol), Fourier data were adjusted to a common phase origin with the program ORIGTILT using reflections with IQ ≤ 3 (S/N = 4.1) for freeze-dried crystals and IQ ≤ 2 (S/N = 8.2) for wormlike crystals. For wormlike crystals, we used additional constraints of symmetry during this phase origin refinement: p2 symmetry for the (*h*,0,*l*) projection and cm symmetry for the (*h*,*k*,0) projection. Data were then averaged by performing a vector addition of individual phases weighted according to their IQ value (Henderson et al., 1986); for freeze-dried crystals, data with IQ ≤ 5 were used, whereas with wormlike crystals data with IQ ≤ 4 were used. A figure of merit (FOM) was derived from each vector addition and served both as an estimate of the phase error ($\cos^{-1}$(FOM)) and as a weight for calculation of the corresponding map. In the case of wormlike crystals, symmetry-related phase residuals were calculated as $\Sigma|F_i|\ |\varphi_i - \varphi_{sym}|/\Sigma|F_i|$, where $|F_i|$ represents the amplitude, φ_i represents the phase of reflections from individual images after phase origin adjustment, and φ_{sym} represents the closest symmetry-constrained phase. Furthermore, for these frozen-hydrated crystals, we included data from both levels of defocus (~8000 Å and ~1.6 μm) in the average and did not correct for the contrast transfer function, although only data within the first zero was used; this combined contrast transfer function is much flatter than that from a single image and therefore reasonably represents Fourier data across a wide range of resolutions (Toyoshima and Unwin, 1988).

X-ray diffraction

Low-angle x-ray diffraction was recorded from wormlike crystals grown in both 20% and 5% glycerol. After crystallization and characterization by negative stain electron microscopy, 100 μg crystallized protein was placed in a 1-mm glass capillary without dilution or any other manipulation. Crystals were then allowed to settle naturally for 2–4 weeks until a pellet was obtained in the capillary. Excess solution was removed, and the capillary was sealed with wax. Diffraction was collected during 12–60-h exposures on CEA reflex x-ray film with Cu K_α x-rays generated with a Rigaku RU-2000 (Rigaku USA, Danvers, MA) rotating anode selected with a graphite monochromator and a 0.4-mm collimator. Helium-filled beam tunnels were used to reduce background scatter, and the crystal-to-film distance was ~480 mm, thus yielding a resolution range of 210–50 Å.

RESULTS

Packing normal to the lamellar plane

To investigate unit cell parameters normal to the lamellar plane, we prepared frozen-hydrated samples of small, wormlike crystals. Because of their shape, these crystals lie with their *c* axis parallel to the plane of the specimen support, and stacking of the lamellae is therefore directly visible. In some cases, the (*h*,0,*l*) projection was obtained, and optical diffraction was then visible to ~25 Å resolution (Fig. 2). Normally, crystals are grown in a solution containing 20% glycerol, and because this was too viscous for efficient blotting, the glycerol concentration was lowered before freezing either by dialysis or by dilution. However, these small crystals were susceptible to becoming disordered, especially after extended dialysis, and dilution reduced the number of crystals present on the specimen support; therefore, crystals were also grown in solutions containing only 5% glycerol, which required less dilution before freezing. However, we found that unit cell parameters measured from crystals grown in 20% glycerol were different from those grown in 5% glycerol. Specifically, we measured the length of the *c* axis as 184.7 Å (SD 1.4 Å, n = 5) in 20% glycerol compared to 161.0 Å (SD 1.5 Å, n = 7) in 5% glycerol. The angle β (see Fig. 1) also appeared to be slightly different: 94.7° (SD 0.6°) and 98.3° (SD 0.8°), respectively. Despite these differences, the spacings along the *a* axes were indistinguishable: 168.8 Å (SD 0.8 Å) and 167.2 Å (SD 2.4 Å), respectively. Furthermore, the resolution obtained from the two categories of crystals was comparable: ~20 Å, judging from phase residuals during merging of the data from the groups of images (8.3° for 9 images from 20% glycerol and 8.7° for 13 images from 5% glycerol). In both cases, the expected p2 symmetry also seemed to be preserved to a comparable extent (p2-related phase residuals of 12.3° and 14.0°, respectively).

Averaged projection maps for these two categories of crystals are shown in Fig. 3. They are both characterized by a homogeneous band of high density running parallel to the *a* axis, which we presume to be the bilayer. In maps from crystals in 20% glycerol, there is little overlap of cytoplasmic heads protruding from apposing layers (see Fig. 1), and individual molecules can therefore be easily distinguished (shading in Fig. 3); the size of this shaded structure is consistent with the previously determined size of these heads (height of 70 Å from the bilayer surface; Toyoshima et al., 1993), and the ~140 Å of space between bilayer surfaces in these crystals (assuming a 45-Å-thick bilayer) leaves sufficient room for their packing. Based on maps from freeze-dried crystals (see below and Fig. 6), it is likely that the smaller domain on the left side of the shaded density corresponds to the "nose" or "beak" of the cytoplasmic head. Furthermore, the "stalk" that connects this head to the bilayer likely corresponds to the narrow region of density between the head and the bilayer.

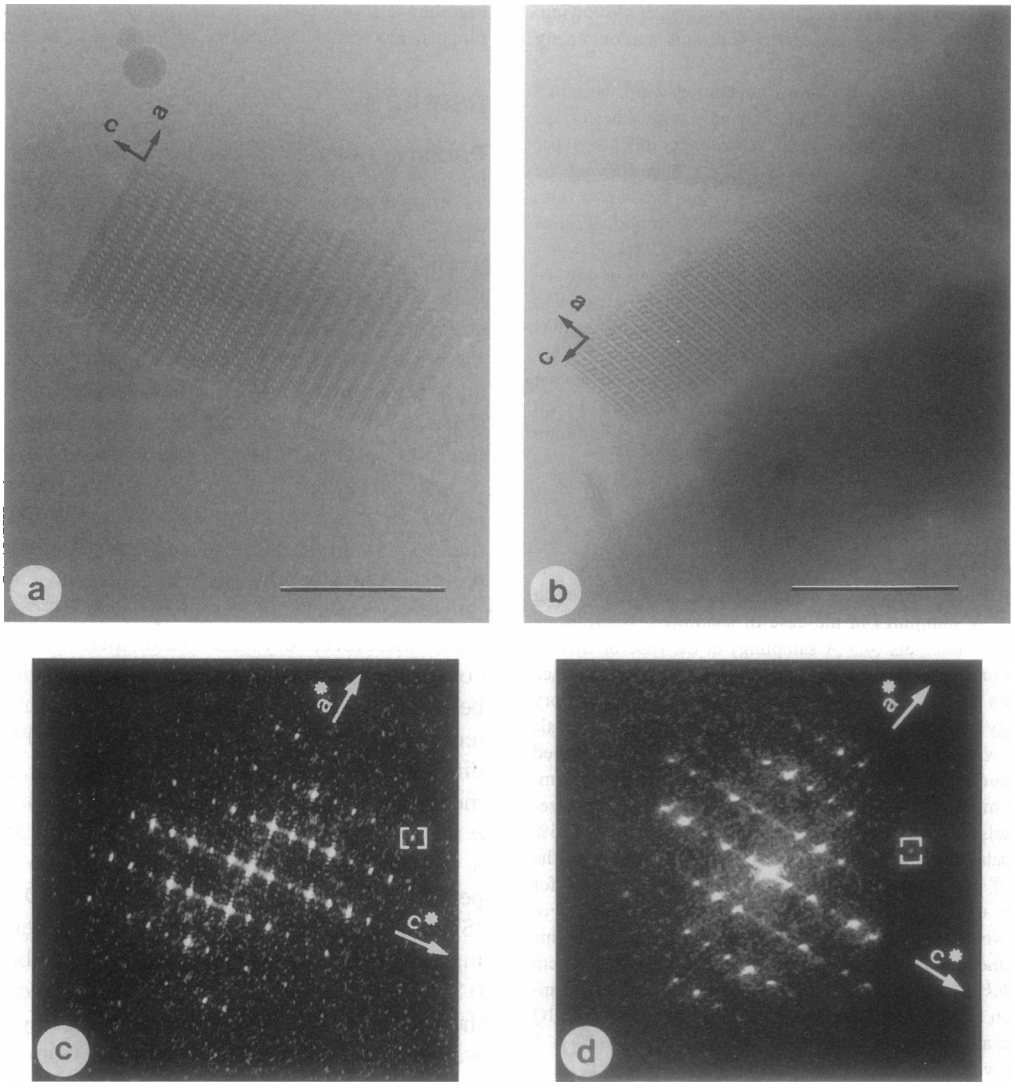

FIGURE 2 Small, wormlike crystals preserved in the frozen-hydrated state. Stacking of the lamellae is directly visible in these crystals, and occasionally the (h, 0, l) projection is obtained, from which the angle β can be measured. *a* and *c* correspond to an image and computed diffraction from crystals grown in 20% glycerol; *b* and *d* are from crystals grown in 5% glycerol. In both cases, reflections are seen to a resolution of ~25 Å (brackets in *c* and *d*). Note that in this space group (C2), reflections $h + k = 2n$ are systematically absent; therefore, the apparent spacing along the *a* axis is 83 Å instead of 166 Å. Scale bars in *a* and *b* represent 0.2 μm.

In contrast, crystals grown in 5% glycerol have only ~115 Å between bilayer surfaces, and as a result, there is evidence of significant overlap of the cytoplasmic heads in the projection maps (Fig. 3). Because of this overlap, some of the highest density in these maps occurs half-way between the bilayers, which is a region of quite low density in maps from crystals in 20% glycerol. Using the basic molecular profile from crystals in 20% glycerol, we have constructed a packing scheme (Fig. 3, *inset*) that accounts reasonably well for density in these projection maps. Unlike the map shown, we initially chose a unit cell with $\beta = 98°$ for crystals in 5% glycerol, but the molecules appeared to have the opposite hand relative to those from 20% glycerol with $\beta = 95°$; i.e., the nose faced in the opposite direction. Therefore, we inverted the *a* axis, which made $\beta = 82°$ as shown in Fig. 3 for crystals from 5% glycerol, thus generating a consistent handedness for the molecule in the two maps. In support of this assignment, the spatial relationship between molecules related by the twofold screw axis is consistent in the two maps shown in Fig. 3: the molecule below the bilayer is displaced slightly to the right relative to the one above the bilayer. This displacement is reversed when the hand of one map is reversed and, if adopted, would thus imply a very different packing of molecules within the lamellar plane. Even after choosing the correct hand for the maps in Fig. 3, the magnitude of the displacement is a little larger in crystals from 5% glycerol.

Packing within the lamellar plane

To address directly the in-plane packing, we analyzed images of collapsed wormlike crystals, which sometimes yield

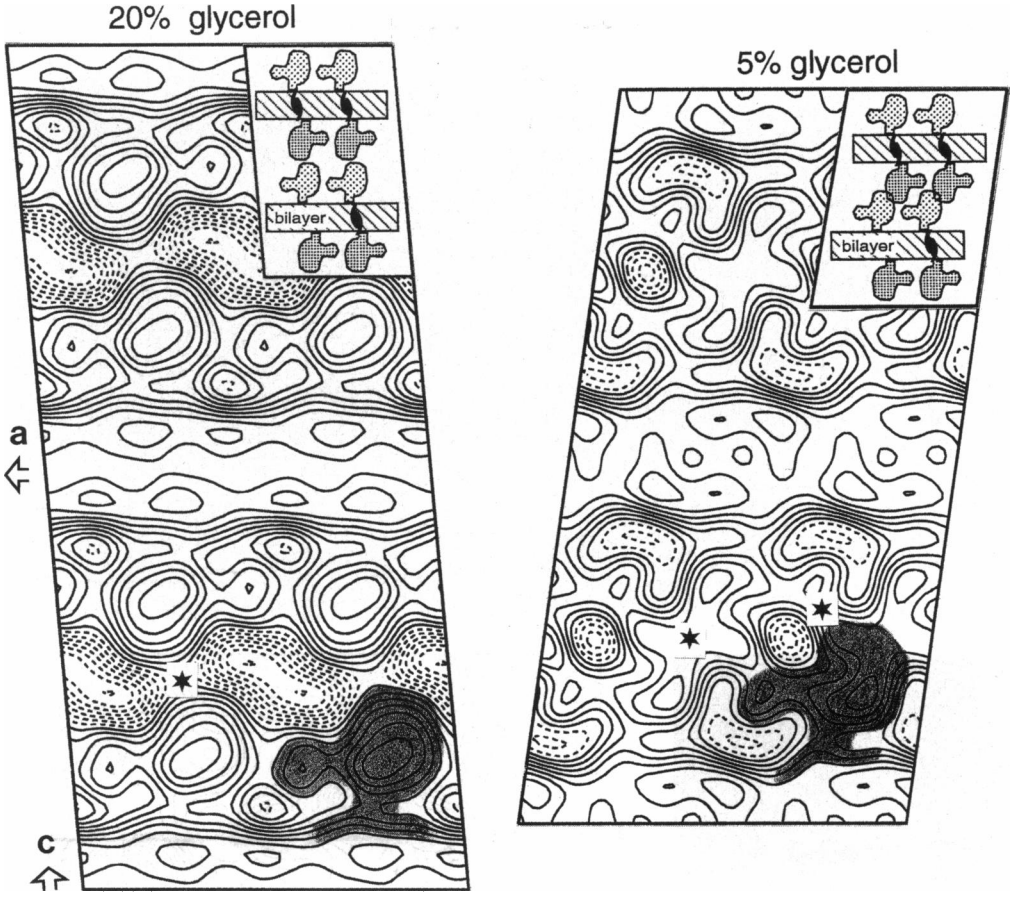

FIGURE 3 Projection maps of wormlike crystals grown in 20% and 5% glycerol. In both maps, the area corresponding to a single cytoplasmic head has been shaded in the lower right corner. The stars show possible intermolecular contacts that stabilize the lamellar stacking. (*Inset*) Cartoons depicting the proposed packing of molecules in the two crystals; twofold screw axes shown do not fully describe crystal symmetry (see Fig. 1) but define twofold screw-related molecules described in the text.

views normal to the lamellae ((*h*,*k*,0) projection, *arrow* in Fig. 4). Such views are comparable to those of untilted platelike crystals (Fig. 5), allowing us to verify unit cell dimensions within the lamellar plane (*a* and *b*) and to calculate the corresponding projection map. The cell dimensions we measured from seven collapsed wormlike crystals grown in 20% glycerol were indistinguishable from those previously determined from platelike crystals: $a = 168.8$ Å (SD 2.9) and $b = 56.5$ Å (SD 0.6), which are both 1.4% larger than previously measured and could therefore be explained by a slight difference in magnification. Furthermore, the measured included angle of $\gamma = 89.7°$ (SD 0.3) is very close to the expected 90° angle for a centered lattice. Unfortunately, we did not find the (*h*,*k*,0) projection for crystals in 5% glycerol, though x-ray diffraction is consistent with these same in-plane spacings (see below).

In addition to these unit cell dimensions, the projection map from these collapsed crystals (Fig. 4) is very similar to analogous maps calculated from thin, platelike crystals (Stokes and Green, 1990a,b). In particular, there are four main densities in the unit cell, which are lined up in rows parallel to the *b* axis, which were also seen in previous maps of negatively stained crystals at a comparable resolution (*h*,*k*,0 projection in figure 6 of Stokes and Green, 1990b). The map in Fig. 4 also has a general resemblance to those from frozen-hydrated crystals (figure 5, *a* and *b*, in Stokes and Green, 1990a), although the details are a little different, probably because of factors such as contrast transfer function, temperature factor, and the fact that $\beta \neq 90°$.

Thus, it seems likely that the molecular packing within the lamellar plane is the same in platelike crystals and wormlike crystals grown in 20% glycerol. This is probably also true for wormlike crystals in 5% glycerol, given that the *a* and *b* dimensions are the same. The slightly larger displacement between twofold screw-related molecules in 5% glycerol (Fig. 3) leaves open the possibility of a small change in packing within the bilayer, but the constancy of unit cell dimensions both in x-ray patterns and in images suggests that any such changes are minor.

To further define the orientation of molecules within the lamellae, we prepared freeze-dried, shadowed crystals, thus revealing only the surface of the crystals (i.e., top half of the unit cell shown in Fig. 1). A proposal for this orientation was previously made based on space considerations within the unit

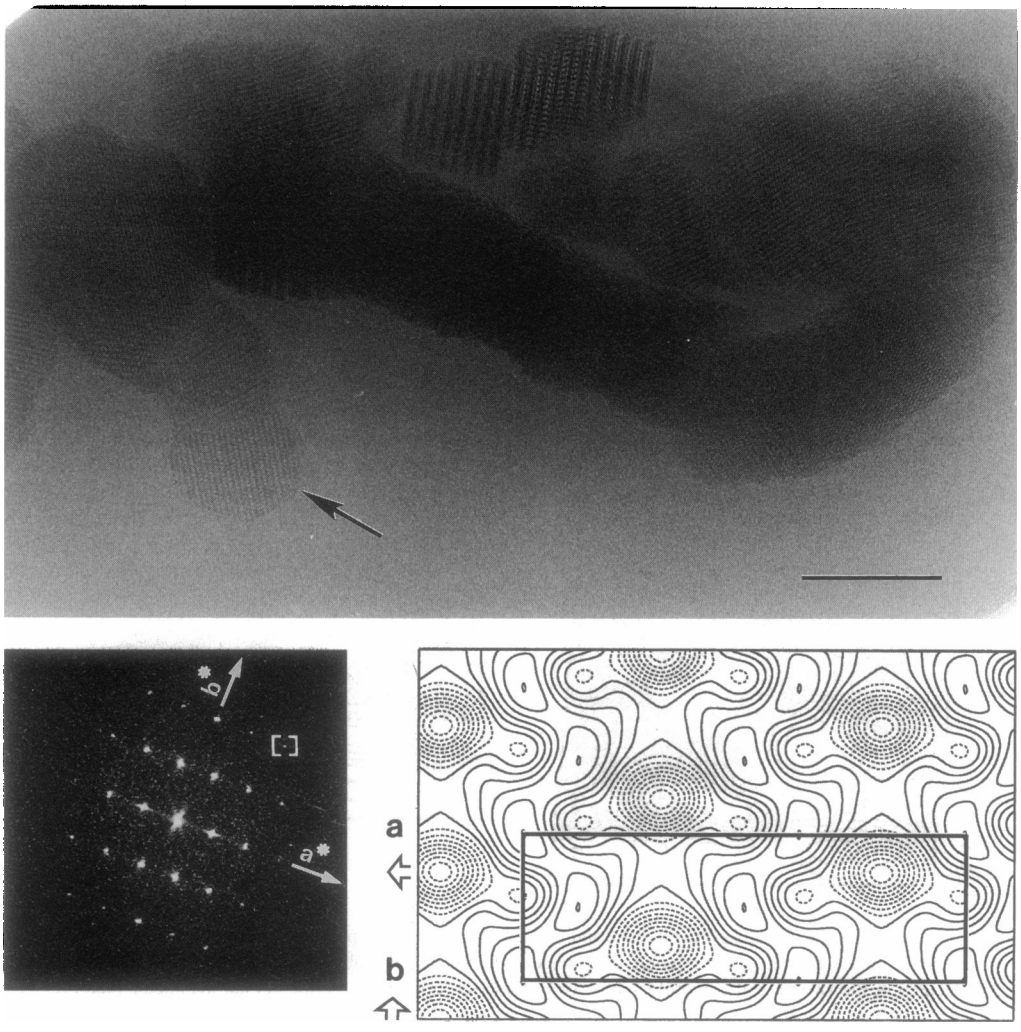

FIGURE 4 A collapsed, wormlike crystal grown in 20% glycerol in which the (h, k, 0) projection (normal to the lamellae) is visible (*arrow*). This crystal has adsorbed to the carbon film, unlike those in Fig. 4, which are suspended in buffer over holes in this film, and the adsorption probably contributes to crystal collapse. The computed diffraction from this (h, k, 0) projection reveals a centered lattice with the expected periodicities, and reflections to 22 Å resolution (*brackets*) show cm symmetry (i.e., reflections with $h + k$ = odd integers are systematically absent and $F(h, k) = F(-h, k)$). The projection map was obtained after averaging seven images (merging phase residual of 8.5°) and enforcing cm symmetry (symmetry-related phase residual of 24.4°). The resulting distribution of density is consistent with that previously obtained from frozen-hydrated, platelike crystals (Stokes and Green, 1990a).

cell (Stokes and Green, 1990b), but superposition of density in projection maps left considerable uncertainty. A shadowed, freeze-dried crystal is shown in Fig. 5 along with its Fourier transform. The crystal shows the expected spacings along the *a* and *b* crystal axes, and steps in crystal thickness along *c* are also clearly visible (*arrowhead*). Computed Fourier transforms from digitized images showed strong, blurred spots to ~40 Å resolution, but after correcting lattice defects, Fourier data were recovered to ~30 Å resolution. Data from eight images were then adjusted to a common phase origin, and data were merged together, assuming p1 symmetry to yield a final phase residual of 7.3°. As expected, the cm symmetry of the projection along the *c* axis was not observed (Fig. 6), because the replicas only represent the top half of the unit cells. This observation is consistent with the lack of negative stain contrast from internal portions of the crystals, even though we washed them with low concentrations of uranyl acetate (0.1–0.2%) before freezing. Nevertheless, we have indicated the unit cell corresponding to the C2 space group for consistency with previous work. The resulting map (Fig. 6) shows triangle-shaped structures that we believe correspond to the cytoplasmic domain of individual Ca^{2+}-ATPase molecules. This domain is known to have a "nose" or a "beak" that confers asymmetry (Taylor et al., 1986; Toyoshima et al., 1993), and our map suggests that this nose is oriented parallel to the *a* axis, which is consistent with the previously proposed packing diagram shown in Fig. 1.

X-ray diffraction

Pellets of wormlike crystals were prepared by natural sedimentation of crystals in their mother liquor, and x-ray

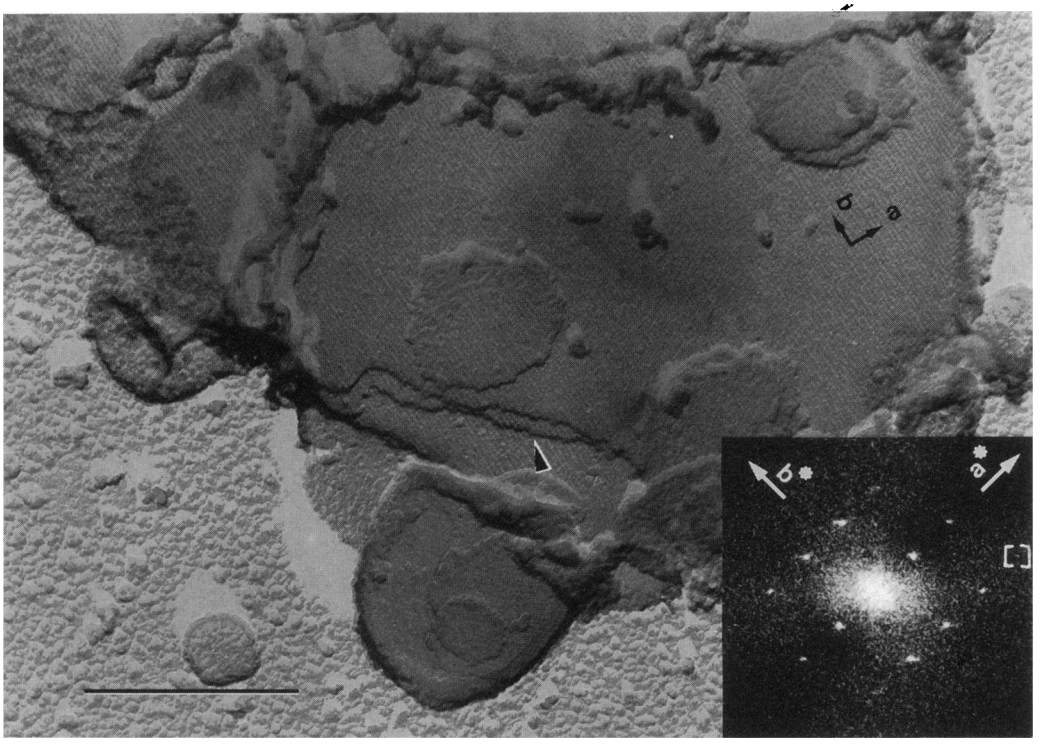

FIGURE 5 Freeze-dried, shadowed platelike crystals. The periodicities seen in the image come from molecules protruding from the topmost surface of the crystal. The stacking of lamellae is visible (*arrowhead*), and the consistency of the lattice in the various layers indicates that these lamellae stack in register to produce a true three-dimensional crystal. The computed diffraction pattern (*inset*) comes from a small area with no lamellar steps after correcting lattice distortions in the original image; reflections are visible to a resolution of ~28 Å (*brackets*). The direction of shadowing is toward 11 o'clock (i.e., direction of the *arrowhead*), and the scale bar represents 0.3 μm.

powder patterns were recorded in an attempt to verify the unit cell spacings observed by electron microscopy. Fig. 7 shows x-ray patterns from crystals grown both in 20% and in 5% glycerol, together with a radial integration of intensity. Table 1 lists the spacings of the various rings and attributes them to reflections either along the lamellar axis (0,0,*l*) or within the lamellar plane (*h*,*k*,0). We found strong rings at each of the spacings expected for low-order, in-plane reflections (~83 Å for the 2,0,0; ~53 Å for the 1,1,0; ~40 Å for both the 4,0,0 and the 3,1,0), consistent with the idea that in-plane cell dimensions are the same for all crystal forms: wormlike crystals grown in 20% or 5% glycerol and platelike crystals. In addition, several reflections were consistent with the lamellar spacings observed by electron microscopy. For crystals grown in 20% glycerol, the first ring was rather broad and slightly closer to the origin than the expected spacing of 83 Å. Given the electron microscopic evidence for a lamellar spacing of 185

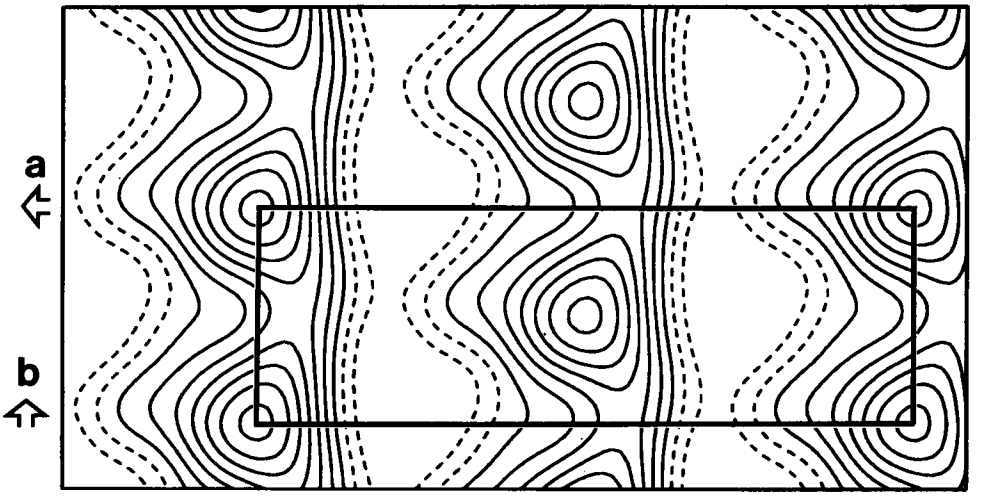

FIGURE 6 Averaged density map from freeze-dried, shadowed crystals. Rows of density correspond to rows of molecules along the *b* axis in Fig. 1. Because shadowing only reveals molecules from the topmost crystal surface, only two molecules are expected per centered unit cell; therefore, each triangular density corresponds to one molecule protruding from the top surface of the crystal. Given the known structure of Ca^{2+}-ATPase, the triangular shape indicates that the nose of the molecule is, in fact, oriented parallel to the *a* axis.

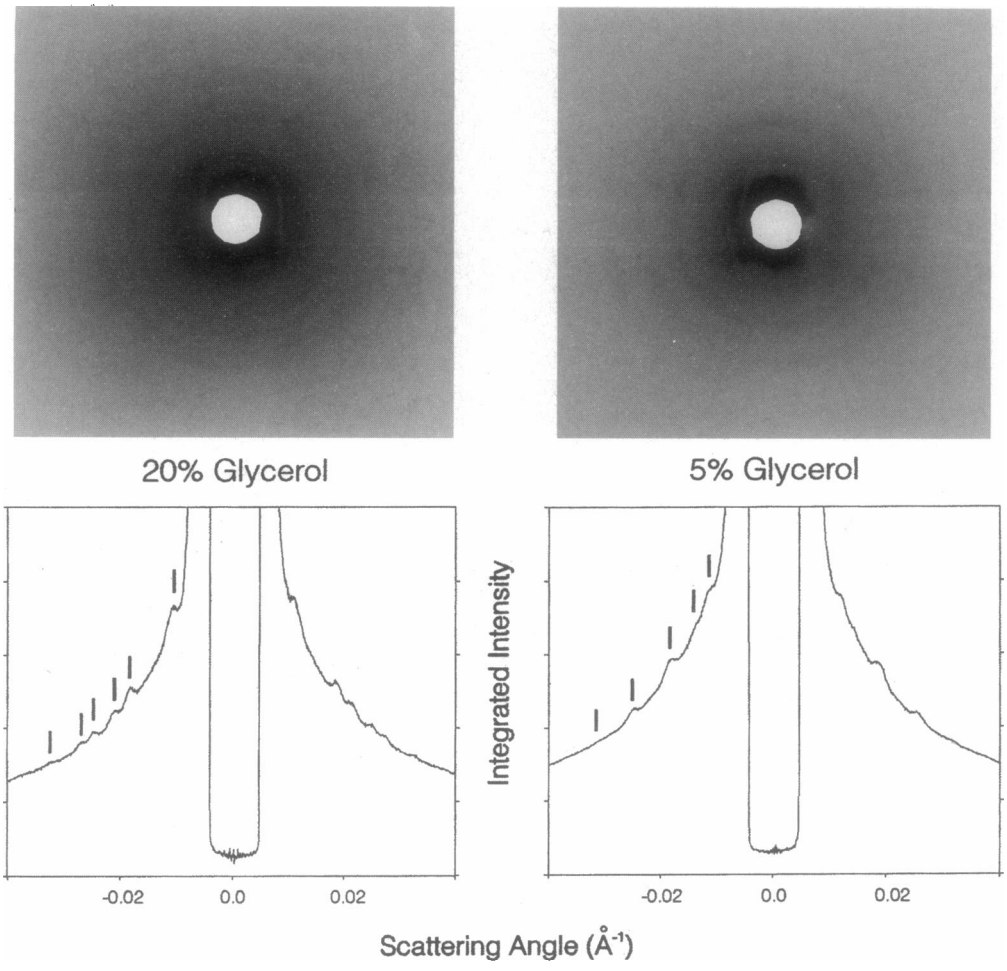

FIGURE 7 X-ray diffraction from pellets of crystals grown in 20% or 5% glycerol. The crystals were not centrifuged, but allowed to settle naturally in capillaries, and no orientation is therefore observed. The lower panels are the radial integration of the corresponding x-ray diffraction patterns. Spacings of individual rings were measured after radial integration and background subtraction. The vertical bars in the lower panels indicate the rings detected for these particular patterns; for 20% glycerol, bars are at 87.7, 53.7, 47, 39.9, 37, and 30.7 Å, and for 5% glycerol, bars are at 83, 71, 53.6, 39.6, and 31.8 Å. Assignments for these rings are given in Table 1.

Å, we believe that this first ring likely consists of two unresolved rings at 92.5 Å (0,0,2) and 83 Å (2,0,0), which is supported by the presence of two higher angle rings at spacings consistent with (0,0,5) and (0,0,6) reflections. Patterns from crystals grown in 5% glycerol were significantly different. In particular, the lowest angle ring is sharper and appears exactly at 83 Å; furthermore, a higher angle reflection is uniquely consistent with a lamellar spacing of 159.7 Å, which after accounting for $\beta = 98°$, corresponds to a spacing along c of 161 Å. In both cases, the two rings at ~70 Å and at ~47 Å probably do not come from the crystals; the relative intensities of these rings were variable (sometimes zero), and they were observed in diffraction from platelike crystals (unpublished observations). The platelike crystals were partially oriented, and these extra rings were seen along the equatorial axis; they therefore cannot be associated with lamellar stacking. Because they do not correspond with any known in-plane reflections, we assume that they arise from some lipid/detergent structure coexisting with crystals.

DISCUSSION

Glycerol affects stacking of lamellae

We set out to determine the unit cell parameters normal to the lamellar plane and to assess the possibility of using small, wormlike crystals in our three-dimensional reconstruction to supplement data from tilted, platelike crystals. For this purpose, wormlike crystals must adopt the same crystal packing as large, platelike crystals. However, we have observed significant differences in the stacking of lamellae, which suggest that molecular packing is in fact variable. These differences cannot be explained by crystal misorientation because the expected p2 symmetry of the $(h,0,l)$ projection was observed in both cases and would not be present in other views of the C2 space group. Furthermore, preparation for electron microscopy (i.e., dilution and freezing) are unlikely to be responsible for the differences, as low-angle, x-ray diffraction data of unperturbed crystals are consistent with electron micrographs. Despite these dif-

TABLE 1 Spacings and assignments for low-angle x-ray diffraction*

20% glycerol			5% glycerol		
Spacing	Assignments‡		Spacing	Assignments§	
(Å)	(0, 0, *l*)	(*h*, *k*, 0)	(Å)	(0, 0, *l*)	(*h*, *k*, 0)
87.7¶	(0, 0, 2)	(2, 0, 0)	83.3	—	(2, 0, 0)
67.1‖	—	—	71.1‖	—	—
53.7	—	(1, 1, 0)	53.6	(0, 0, 3)	(1, 1, 0)
47.0‖	(0, 0, 4)	—	46.4‖	—	—
39.9	—	(4, 0, 0); (3, 1, 0)	39.6	(0, 0, 4)	(4, 0, 0); (3, 1, 0)
37.0	(0, 0, 5)	—			
30.7	(0, 0, 6)	—	31.8	(0, 0, 5)	—
26.7	(0, 0, 7)	(2, 2, 0)	26.9	(0, 0, 6)	(2, 2, 0)
23.5	(0, 0, 8)	(4, 2, 0)			

* Measurements represent an average of x-ray patterns collected from three individual pellets.

‡ Assignments for crystals grown in 20% glycerol are consistent with a lamellar spacing of 185.3. Å and in-plane spacings of a = 166.4 Å and b = 55.7 Å.

§ Assignments for crystals grown in 5% glycerol are consistent with a lamellar spacing of 159.7 Å and in-plane spacings of a = 166.4 Å and b = 55.7 Å.

¶ This strong reflection was broader than other assigned reflections and is therefore consistent with an unresolved doublet of the (0, 0, 2) at 92.5 Å and the (2, 0, 0) at 83 Å.

‖ The intensities of these reflections were variable, generally weaker and broader than other reflections; we therefore believe that they come from a noncrystalline component in the solution.

ferences in stacking of lamellae, unit cell dimensions within the lamellar plane are the same in all of the various crystals, and projection maps of collapsed wormlike crystals in 20% glycerol are very similar to maps from platelike crystals. It is therefore likely that molecular packing within the bilayer is the same, and that growth conditions simply affect the interactions between apposing lamellae.

In particular, the concentration of glycerol present during crystallization appears to be responsible for the observed differences in lamellar stacking. We previously found that glycerol had dramatic effects on crystal growth (Shi et al., 1995); for example, 40% glycerol prevented crystal nucleation altogether. Furthermore, after nucleation in 20% glycerol, an increase to 40% glycerol induced crystal fusion and decreased the average number of layers in individual crystals, thus generating a large, thin, platelike morphology. Based on these and other observations, we proposed that nucleation is intimately associated with stacking and that one effect of 40% glycerol is to interfere with this stacking. Our current observations of the effects of glycerol concentration on stacking are consistent with this hypothesis, because the lowest glycerol concentration (5%) promotes the most extensive interaction between the lamellae. Thus, the 185 Å spacing in 20% glycerol may represent an intermediate between the 161 Å spacing in 5% glycerol and complete inhibition of stacking by 40% glycerol.

To define these interlamellar interactions in greater detail, consider the close-packed rows of molecules along the b axis in Fig. 1 (also visible in Fig. 6). Stacking of lamellae in 20% glycerol seems to be accomplished by interactions only between two rows in apposing layers: one upward-facing row and one downward-facing row interacting at the topmost surface of the Ca^{2+}-ATPase molecule (*star* in Fig. 3). In contrast, 5% glycerol appears to promote interactions between a given downward-facing row and two upward-facing rows (*pair of stars* in Fig. 3); the second interlamellar contact links the nose of the downward-facing molecule to the top of the upward-facing molecule, although we cannot be certain of these intermolecular contacts based on projection maps alone.

Packing in wormlike versus platelike crystals

It has previously been assumed that these small, wormlike crystals had the same molecular packing as the large, platelike crystals, because of similar growth conditions and general appearance (Stokes and Green, 1990b). Indeed, it appears likely that molecular packing within the lamellar plane is the same, based on images of collapsed wormlike crystals showing the (*h*,*k*,0) projection (Fig. 4) and on the presence of strong x-ray diffraction at expected spacings for in-plane reflections (Table 1). However, given that stacking of lamellae depends on growth conditions, it is essential to determine the lamellar spacing for the large, platelike crystals that are being used for three-dimensional reconstruction. Previous, low-angle x-ray diffraction showed a spacing of 164 Å normal to the lamellar plane from a pellet of crystals grown in 20% glycerol (Stokes and Green, 1990b), although there are now several reasons to question this result: 1) the presence of platelike and wormlike crystals in this pellet was not determined, 2) crystals were centrifuged at 3000 × g to prepare the pellet, perhaps affecting the lamellar spacing, and 3) the observed single reflection at 1/164 $Å^{-1}$ was very broad relative to in-plane reflections. Recent x-ray diffraction indicates that very large, platelike crystals have a lamellar spacing of 155 Å, and this spacing is consistent both with electron diffraction analysis of tilt series from single crystals and with atomic force microscopy (unpublished results). Thus, the platelike crystals may have yet another scheme for stacking the lamellae.

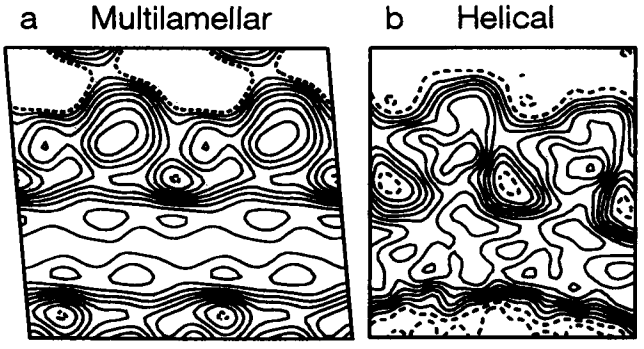

FIGURE 8 Comparison of projection structures from multilamellar crystals (*a*) and helical tubes (*b*). The projection from multilamellar crystals grown in 20% glycerol has been taken from Fig. 3. The projection from helical tubes was calculated from the three-dimensional structure (Toyoshima et al., 1993) from an angle perpendicular to the nose of the molecule (i.e., perpendicular to the "dimer ribbons" composing the helical tubes). Based on the map from freeze-dried, shadowed crystals (Fig. 6), the projection from multilamellar crystals represents the analogous view of the molecule. Multilamellar crystals comprise molecules in the calcium-bound state, whereas helical tubes are composed of the calcium-free state (Stokes and Lacapere, 1994); thus, the differences in the projection maps may be due to conformational changes induced by calcium binding to Ca^{2+}-ATPase.

Given these differences in lamellar spacing, it will not be possible simply to combine Fourier data from the wormlike crystals with those from a tilt reconstruction of platelike crystals. Nevertheless, once the lamellar packing in platelike crystals has been determined from a tilt reconstruction, it may be possible to use data from wormlike crystals grown in 20% glycerol by excising a single layer of molecules from the corresponding projection maps (Fig. 3) and artificially repacking them according to the scheme adopted by the platelike crystals. Such extreme measures are probably worthwhile, as data along the lamellar axis are essential in accurately defining the distribution of mass normal to the lamellae. Thus, higher resolution data from these wormlike crystals, such as those recently obtained by Toyoshima et al. (personal communication), may still prove very valuable in structure determination of Ca^{2+}-ATPase.

The calcium-induced conformational change of Ca^{2+}-ATPase

The enzymatic state of Ca^{2+}-ATPase in these multilamellar crystals has been shown to correspond to the calcium-bound form of the molecule $E_1 \cdot Ca_2$, whereas the structure previously determined from vanadate-induced helical tubes corresponds to the distinct enzymatic form often referred to as E_2 (Stokes and Lacapere, 1994). The calcium-induced transition between these two states, $E_2 \rightarrow E_1 \cdot Ca_2$, represents a main event in the catalytic cycle of Ca^{2+}-ATPase and is thought to involve a large conformational change (Bigelow and Inesi, 1992). It will therefore be very interesting to compare three-dimensional structures from these two crystal forms. In the meantime, we can compare the profile of the cytoplasmic head revealed by the $(h,0,l)$ projection of wormlike, multilamellar crystals with the analogous profile obtained from helical tubes (from Toyoshima et al., 1993). The projection map from wormlike, multilamellar crystals grown in 20% glycerol is the best candidate for this comparison, because it presents a clear profile of individual molecules with minimal superposition from neighbors. Based on our map from freeze-dried crystals, we know that this profile represents a view normal to the nose of the molecule, which is the same view used to present the three-dimensional structure of the molecule obtained from helical tubes. The overall molecular dimensions of the head from the two structures are very similar (70 Å high and 70–75 Å long; Fig. 8). The main difference between these two structures is the shape of the nose: it is gently rounded in multilamellar crystals and distinctly triangular in helical tubes. More specifically, the bottom of the nose (nearest the bilayer) is pushed up and flattened in the helical reconstruction to produce this triangular shape. Interestingly, this region was proposed to be the site of ATP binding in the helical reconstruction (Toyoshima et al., 1993), and, if true, this difference in the shape of the nose may reflect conformational changes that would be expected at the ATP site upon the binding of calcium. Differences within the bilayer are not so easily interpretable, as multilamellar crystals have contributions from molecules protruding from both sides of the bilayer and helical tubes do not. Of course, these structural changes will be much better characterized from a full, three-dimensional reconstruction, but this represents the first look at the kind of conformational change that may accompany calcium binding to Ca^{2+}-ATPase.

The authors gratefully acknowledge Margaretta Allietta for freeze-drying and shadowing of crystals and Dan Czajkowsky for recording and processing the resulting images.

This work was supported by National Institutes of Health grant AR40997 to DLS.

REFERENCES

Amos, L. A., R. Henderson, and P. N. T. Unwin. 1982. Three-dimensional structure determination by electron microscopy of two-dimensional crystals. *Prog. Biophys. Mol. Biol.* 39:183–231.

Andersen, J. P., and B. Vilsen. 1994. Structure-function relationships of cation translocation by Ca^{2+}- and Na^+,K^+-ATPases studied by site-directed mutagenesis. *FEBS Lett.* 359:101–106.

Bigelow, D. J., and G. Inesi. 1991. Frequency-domain fluorescence spectroscopy resolves the location of maleimide-directed spectroscopic probes within the tertiary structure of the Ca-ATPase of sarcoplasmic reticulum. *Biochemistry.* 30:2113–2125.

Bigelow, D. J., and G. Inesi. 1992. Contributions of chemical derivatization and spectroscopic studies to the characterization of the Ca^{2+} transport ATPase of sarcoplasmic reticulum. *Biochim. Biophys. Acta.* 1113: 323–338.

Brandl, C. J., N. M. Green, B. Korczak, and D. H. MacLennan. 1986. Two Ca^{++} ATPase genes: homologies and mechanistic implications of deduced amino acid sequences. *Cell.* 44:597–607.

Castellani, L., P. M. Hardwicke, and C. Franzini-Armstrong. 1989. Effect of Ca^{2+} on the dimeric structure of scallop sarcoplasmic reticulum. *J. Cell. Biol.* 108:511–520.

Castellani, L., P. M. Hardwicke, and P. Vibert. 1985. Dimer ribbons in the three-dimensional structure of sarcoplasmic reticulum. *J. Mol. Biol.* 185:579–594.

Clarke, D. M., T. W. Loo, G. Inesi, and D. H. MacLennan. 1989. Location of high affinity Ca^{2+}-binding sites within the predicted transmembrane domain of the sarcoplasmic reticulum Ca^{2+}-ATPase. *Nature.* 339: 476–478.

Dux, L., and A. Martonosi. 1983. Two-dimensional arrays of proteins in sarcoplasmic reticulum and purified Ca^{2+}-ATPase vesicles treated with vanadate. *J. Biol. Chem.* 258:2599–2603.

Dux, L., S. Pikula, N. Mullner, and A. Martonosi. 1987. Crystallization of Ca^{2+}-ATPase in detergent-solubilized sarcoplasmic reticulum. *J. Biol. Chem.* 262:6439–6442.

Dux, L., K. A. Taylor, H. P. Ting-Beall, and A. Martonosi. 1985. Crystallization of the Ca^{2+}-ATPase of sarcoplasmic reticulum by calcium and lanthanide ions. *J. Biol. Chem.* 260:11730–11743.

Eletr, S., and G. Inesi. 1972. Phospholipid orientation in sarcoplasmic reticulum membranes: spin-label ESR and proton NMR studies. *Biochim. Biophys. Acta.* 282:174–179.

Green, N. M. 1992. Evolutionary relationships within the family of P-type cation pumps. *Ann. N.Y. Acad. Sci.* 671:104–112.

Henderson, R., J. M. Baldwin, T. A. Ceska, F. Zemlin, E. Beckmann, and K. H. Downing. 1990. Model for the structure of bacteriorhodopsin based on high-resolution electron cryo-microscopy. *J. Mol. Biol.* 213: 899–929.

Henderson, R., J. M. Baldwin, K. H. Downing, J. Lepault, and F. Zemlin. 1986. Structure of purple membrane from *Halobacterium halobium*: recording, measurement and evaluation of electron micrographs at 3.5 Å resolution. *Ultramicroscopy.* 19:147–178.

Herbette, L., P. DeFoor, S. Fleischer, D. Pascolini, A. Scarpa, and J. K. Blasie. 1985. The separate profile structures of the functional calcium pump protein and the phospholipid bilayer within isolated sarcoplasmic reticulum membranes determined by X-ray and neutron diffraction. *Biochim. Biophys. Acta.* 817:103–122.

Inesi, G., L. Lu, M. E. Kirtley, and K. Takeyasu. 1994. Distinct structural identities of catalytic and Ca^{2+} binding domains in the sarcoplasmic reticulum ATPase. *Cell Physiol. Biochem.* 4:135–147.

MacLennan, D. H., C. J. Brandl, B. Korczak, and N. M. Green. 1985. Amino-acid sequence of a Ca^{2+} + Mg^{2+}-dependent ATPase from rabbit muscle sarcoplasmic reticulum, deduced from its complementary DNA sequence. *Nature.* 316:696–700.

Pikula, S., N. Mullner, L. Dux, and A. Martonosi. 1988. Stabilization and crystallization of Ca^{2+}-ATPase in detergent-solubilized sarcoplasmic reticulum. *J. Biol. Chem.* 263:5277–5286.

Shi, D., H.-H. Hsiung, R. C. Pace, and D. L. Stokes. 1995. Preparation and analysis of large, flat crystals of Ca^{2+}-ATPase for electron crystallography. *Biophys. J.* 68:1152–1162.

Stokes, D. L., and N. M. Green. 1990a. Structure of CaATPase: electron microscopy of frozen-hydrated crystals at 6 Å resolution in projection. *J. Mol. Biol.* 213:529–538.

Stokes, D. L., and N. M. Green. 1990b. Three-dimensional crystals of Ca-ATPase from sarcoplasmic reticulum: symmetry and molecular packing. *Biophys. J.* 57:1–14.

Stokes, D. L., and J.-J. Lacapere. 1994. Conformation of Ca^{2+}-ATPase in two crystal forms: effects of Ca^{2+}, thapsigargin, AMP-PCP, and Cr-ATP on crystallization. *J. Biol. Chem.* 269:11606–11613.

Stokes, D. L., W. R. Taylor, and N. M. Green. 1994. Structure, transmembrane topology and helix packing of P-type ion pumps. *FEBS Lett.* 346:32–38.

Taylor, K. A., L. Dux, and A. Martonosi. 1986. Three-dimensional reconstruction of negatively stained crystals of the Ca^{++}-ATPase from muscle sarcoplasmic reticulum. *J. Mol. Biol.* 187:417–427.

Taylor, K. A., N. Mullner, S. Pikula, L. Dux, C. Peracchia, S. Varga, and A. Martonosi. 1988. Electron microscope observations on Ca^{2+}-ATPase microcrystals in detergent-solubilized sarcoplasmic reticulum. *J. Biol. Chem.* 263:5287–5294.

Taylor, W. R., and N. M. Green. 1989. The predicted secondary structures of the nucleotide-binding sites of six cation-transporting ATPases lead to a probable tertiary fold. *Eur. J. Biochem.* 179:241–248.

Toyoshima, C. 1989. On the use of holey grids in electron crystallography. *Ultramicroscopy.* 30:439–444.

Toyoshima, C., H. Sasabe, and D. L. Stokes. 1993. Three-dimensional cryo-electron microscopy of the calcium ion pump in the sarcoplasmic reticulum membrane. *Nature.* 362:469–471.

Toyoshima, C., and N. Unwin. 1988. Contrast transfer for frozen-hydrated specimens: determination from pairs of defocused images. *Ultramicroscopy.* 25:279–292.

Unger, V. M., and G. F. X. Schertler. 1995. Low resolution structure of bovine rhodopsin determined by electron cryo-microscopy. *Biophys. J.* 68:1776–1786.